Available online at www.sciencedirect.com

ScienceDirect

Procedia Engineering 138 (2016) 390 – 402

Procedia Engineering

www.elsevier.com/locate/procedia

"SYMPHOS 2015", 3rd International Symposium on Innovation and Technology in the Phosphate Industry

Crystallization of Calcium Sulphate during Phosphoric Acid Production: Modeling Particle Shape and Size Distribution

Zhilong Zhu[a], You Peng[a], T. Alan Hatton[a], Kamal Samrane[b], Allan S. Myerson[a], and Richard D. Braatz[a,*]

[1]*The OCP-MIT Program in Phosphate Processing, Department of Chemical Engineering, Massachusetts Institute of Technology, Cambridge, MA 02139 USA*

[2]*OCP Group, Research & Development Direction, Jorf Lasfar, P.B 118, El Jadida, Morocco*

Abstract

A key unit operation in the production of phosphoric acid is the filtration needed to separate calcium sulphate dihydrate ($CaSO_4 \cdot 2H_2O$, gypsum) crystals from an acid slurry. The filtration efficiency depends on the shape and size distribution (SSD) of the gypsum crystals produced from the upstream reactive crystallization. This article describes the construction of a first-principles model and computationally efficient numerical solver for the prediction of SSD during the reactive crystallization of gypsum while taking non-ideal phase equilibria and the effects of impurities (i.e., metal ions) into account.

A population balance model couples the impurity compositions in the feed streams to the SSD for given process conditions, with the independent dimensions of the crystals being their length and width. Such a population balance model with two independent dimensions is able to represent rod-like crystals with varying aspect ratios (length/width). The compositions of all species in solution and the supersaturation driving force for crystal nucleation and growth are described using a mixed solvent electrolyte model that accounts for long-range, short-range, and ionic interactions. OLI software for computing the compositions is integrated with a Matlab implementation of the population balance model that is solved using the method of characteristics, which transforms the partial differential equations of the population balance model into a system of ordinary differential equations. This simulation method does not exhibit the numerical diffusion or dispersion common in other simulation methods, while being more computationally efficient.

* Corresponding author. Tel.: +1-617-253-3112; fax: +1-617-258-5042.
E-mail address: braatz@mit.edu

Peer-review under responsibility of the Scientific Committee of SYMPHOS 2015
doi:10.1016/j.proeng.2016.02.098

The crystal nucleation and growth rates are measured in a series of mixed-suspension mixed-product-removal experiments of various acid concentration, temperature, and impurity levels. A variety of models for the effects of impurities on the growth rates along the width and length dimensions are compared in terms of their ability to describe experimental observations.

Peer-review under responsibility of the Scientific Committee of SYMPHOS 2015

Keywords: phosphoric acid; particle shape; crystallization; population balance models; gypsum

1. Introduction

About 90% of the world's phosphate consumption goes directly into the fertilizer industry [1]. Phosphoric acid as the main starting material in the fertilizer manufacturing is produced almost exclusively by the Wet Process [2]. The two main steps in the Wet Process consist of (1) digestion of phosphate rock by concentrated sulfuric acid in the reactor-crystallizer, and (2) recovery of the phosphoric acid from the suspension in the filtration unit. The main reaction in the digestion can be generalized as

$$Ca_3(PO_4)_2 + 3H_2SO_4 \xrightarrow{H_2O} 2H_3PO_4 + 3CaSO_4 \cdot xH_2O \downarrow \quad (1)$$

where x equals 0, 0.5, or 2 depending on the processing technology use. The hemihydrate (x = 0.5) and dihydrate (x = 2) process technologies are both widely used in industrial phosphate production. The choice between the two technologies depends heavily on the phosphate rock quality and the choice of operating temperature. The dehydrate process technology of interest in this study, but the two technologies share many features in common and the modelling approach discussed in this article can be modified to apply to the hemihydrate process as well.

The separation of phosphoric acid from solid gypsum is the bottleneck process [3]. Many plants operate with the production limited by the filtration stage [4]. Crystal shape and size distribution (SSD) are the most important factors that influence the filtration rate and liquid entrainment. Gypsum crystal has a natural tendency to form needle-shaped and tabular crystals in the absence of additives [3]. The cake formed with these crystals has a high filtration resistance, which is not favorable for solid-liquid separation and has motivated research in the upstream reactive crystallization with the objective of modifying the SSD to debottleneck the filtration stage.

This article constructs a first-principles model and computationally efficient numerical solver for the prediction of SSD during reactive crystallization of gypsum while taking nonideal phase equilibria and the effects of impurities (i.e., metal ions) into account.

Nomenclature

a	activity coefficient
b	nucleation rate exponent
B	nucleation rate
B_{ij}	binary interaction parameter between species i and j
c	concentration if the subscript is a species or constant if the subscript is an index
E	activation energy
f	population density function
g	growth rate exponent
G	crystal growth rate
G^{ex}	Gibbs excess energy
H	rate of generation and disappearance of crystals
I_x	ionic strength
k	rate constant for nucleation or growth

k_v	shape factor
K	equilibrium adsorption constant
K_{sp}	solubility product
L	length dimension
Q	volumetric flow rate
r_0	critical nucleus size
R	gas constant
S	supersaturation ratio
t	time
T	temperature
V	reactor volume
W	width dimension
x	mole fraction
α	effectiveness factor in impurity growth model
β	lumped parameter
δ	delta function
θ	impurity surface coverage
μ	chemical potential
μ_3	third moment, which is proportional to the total crystal volume
ν	stoichiometric coefficient in a reaction
ρ	crystal density
σ	relative supersaturation

2. Population balance model

The population balance model (PBM) is the conservation equation for the number of particles [5,6]. The mathematical framework enables the modeling of particle formation, growth, breakage, and aggregation. PBMs have been applied to many particulate systems including crystallizsation, polymerization, multiphase reaction, and biological systems [7]. In the field of precipitation, PBM is used to model the crystal size distribution (CSD) of many systems including sodium salicylate [8], calcium carbonate [9], barium sulfate [10], and silver bromide [11].

When spatial inhomogeneity is not considered, the number of independent dimensions of the crystals specifies the dimension of the population balance model, with most crystals being well modeled as having two dimensions: length L and width W (see Fig. 1). The two-dimensional (2D) transient population balance equation (PBE) for a crystallization with inflow and outflow in a well-mixed system is [6]

$$\frac{\partial f}{\partial t}+\frac{\partial G_L f}{\partial L}+\frac{\partial G_W f}{\partial W}+f\frac{d(\ln V)}{dt}=H\left(f,L,W\right)+\frac{\sum Q_{in} f_{in}-\sum Q_{out} f_{out}}{V} \tag{2}$$

where $f = f(t,L,W)$ is the 2D crystal size distribution (aka population density function), $G = G(L,W)$ is the crystal growth rate in the direction of the subscript, Q is the volumetric flow rate of inlet and outlet stream, and $H(f,L,W)$ is the rate of generation and disappearance of crystal due to nucleation, agglomeration, and breakage. In contrast to the one-dimensional PBE most often used for modeling crystallizations, the 2D PBE is capable of modelling crystal of varying aspect ratio (L/W), which is observed for gypsum crystals.

This article considers secondary nucleation

$$H\left(f,L,W\right)=k_b\sigma^b\mu_3\delta(L,W) \tag{3}$$

as the only particle generation mechanism, where k_b is the rate constant which has Arrhenius temperature dependency, σ is the relative supersaturation, b is the nucleation exponent, and μ_3 is proportion to the total crystal volume and can

be computed from taking the integral of the entire distribution, $\delta(L,W)$ is the 2D Dirac delta function indicating the crystal nuclei have negligible size.

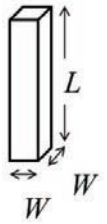

Fig. 1. Crystal dimensions modelled by a 2D PBM to better represent the varying aspect ratio observed in rod-like gypsum crystals.

The population balance model couples solute mass balances with the PBE (2) to track the solution concentration as crystals grow. The mass balances are in the form of algebraic equation or differential equations for either batch or open systems. To complete the PBM, both boundary condition and initial conditions need to be specified.

3. Method of Characteristics

The PBE (2) is first-order hyperbolic partial differential equation (PDE). The mass balance and nucleation term in the PBE are a function of the crystal total mass, which results in the PBE being an integro-partial differential equation. The integral function and the nonlinear expression in the constitutive equations make analytical solution not possible in most cases. In the numerical treatment, the presence of a steep moving front due to the hyperbolic nature of the PBE can cause numerical diffusion and stability issues.

Several numerical methods for solving PBEs are reported in literature [12,13]. One of the most efficient and accurate numerical methods for solving a PBE is the method of characteristics (MOC), which discovers curves along which the PDE becomes ordinary differential equations (ODEs). The solution to the system of ODEs gives the characteristic curves that propagate the size density information, which are used to construct the population density at any given time. Mathematically, the MOC transforms the PBE (2) into a system of ODEs, and the integral into a summation:

$$\frac{\mathrm{d}L_i}{\mathrm{d}t} = G_{L,i} \tag{4a}$$

$$\frac{\mathrm{d}W_j}{\mathrm{d}t} = G_{w,j} \tag{4b}$$

$$\frac{\mathrm{d}f_{ij}}{\mathrm{d}t} = f_{ij}\left(\frac{\mathrm{d}G_{L,i}}{\mathrm{d}L_i} + \frac{\mathrm{d}G_{W,j}}{\mathrm{d}W_j}\right) - f_{ij}\frac{d(\ln V)}{dt} + \frac{\sum Q_{in} f_{in,ij} - \sum Q_{out} f_{out,ij}}{V} \tag{4c}$$

$$\mu_3(t) = \int_0^\infty \int_0^\infty f(t,L,W) L W^2 dL dW \approx \sum_j \sum_i f_{ij} L_i W_j^2 \Delta L_i \Delta W_i \tag{5a}$$

The nucleation term is not included in the above equation as it was implemented instead as a boundary condition. The system of ODEs can be easily solved using commercial solvers such as ode15 in Matlab. The summation in (5a) can be replaced by an alternative summation derived from the midpoint rule or higher order quadrature methods.

3.1. Nucleation implementation in MOC

In the presence of nucleation, new characteristics are defined to account for the newborn nuclei. The model (3) treats nucleation as occuring only at a single point in the size domain defined by the delta function. In reality, crystals

may nucleate over a small range of sizes. To take this into account, the delta function in (3) can be replaced by a normal distribution or polynomial that integrates to 1 over the defined domain. For example, the delta function in (3) could be replaced by

$$\hat{\delta}(L,W)=\begin{cases}\dfrac{9}{8r_0^2}\left(1-\dfrac{16}{r_0^4}\left(L-\dfrac{r_0}{2}\right)^2\left(W-\dfrac{r_0}{2}\right)^2\right), & 0\le L\le r_0,\ 0\le W\le r_0\\ 0, & \text{Otherwise}\end{cases} \tag{5b}$$

Tracking the nucleated crystals in the MOC based on (5b) requires defining $O(N^2)$ number of characteristics, which is computationally expensive especially when simulating a nucleation-dominated crystallization. One way to reduce the number of introduced characteristics is by projecting the nucleated crystal from the 2D size domain to 1D size domain, which is equivalent of having a curve in space, which requires only $O(N)$ number of characteristics. When computing the integral equation in (5b), the area under the curve is computed by projecting the curve to the 1D size domain and computing using quadrature methods like the midpoint rule. A key assumption that allows this simplification is size-independent growth in both directions.

4. Thermodynamics model for solution nonideality

4.1. Gypsum solubility

Gypsum dissociates in the presence of aqueous solution, and its solubility is governed by the equilibrium reaction with its dissociated ions and water molecules. An accurate prediction of gypsum solubility in a concentrated multicomponent electrolyte system requires chemical speciation analysis, which is the determination of all chemical species including ionic, metal-ligand complexes, and undissociated species in the aqueous solution at chemical equilibrium. Variation in the concentration of any species in the solution shifts the chemical equilibria and ultimately affects gypsum solubility.

For higher ionic strength or industrial strength solutions, simplified approaches are not valid for predicting solubility due to severe nonideality resulting from various interactions between the formation of species and complexes. Several model frameworks have been established to estimate the nonideality for concentrated electrolyte systems, including the electrolyte-NRTL model and mixed solvent electrolyte (MSE) model. This study uses the MSE model because it has been demonstrated in the widest range of industrial applications and has been observed to have higher model accuracy than alternative models for many electrolyte systems [14–17].

4.2. Mixed Solvent Electrolyte model

The MSE model [18,19] is a speciation-based model that determines phase equilibrium by performing speciation calculation for all species participating in the chemical equilibria. The speciation calculation in the MSE model relies on the Helgeson-Kirkham-Flowers (HKF) model framework for standard state computation [18]. The excess Gibbs free energy, which describes the solution's nonideality, is modeled based on a combined framework of Debye-Huckle, Bromley, Pitzer, Zemaitis, and others.

Typically, the nonideality of an electrolyte solution arises from various forces including electrostatic (long-range) forces, chemical forces, and physical dispersion forces [19]. While electrostatic forces are usually dominant in dilute solutions, chemical and physical dispersion forces become dominant in concentrated solutions. To account for all these contributions, the excess Gibbs free energy is calculated:

$$G^{\text{ex}}=G_{LR}^{\text{ex}}+G_{II}^{\text{ex}}+G_{SR}^{\text{ex}} \tag{6}$$

where G_{LR}^{ex} is the contribution of long-range electrostatic interactions, G_{II}^{ex} accounts for specific ionic (ion-ion and ion-molecule) interactions, and G_{SR}^{ex} is a short-range contribution resulting from intermolecular interactions. The long-

range interaction contribution is calculated from the Pitzer-Debye-Hückel formula [20] expressed in terms of mole fractions and symmetrically normalized. The short-range interaction contribution is calculated from the UNIQUAC equation [21]. The specific ion-interaction contribution is calculated from an ionic strength-dependent, symmetrical second virial coefficient-type expression [19]:

$$\frac{G_{II}^{ex}}{RT} = -\sum_i n_i \sum_i \sum_j x_i x_j B_{ij}(\mathrm{I}_x) \tag{7}$$

where x is the mole fraction of the species, and B_{ij} is a binary interaction parameter between the species i and j:

$$B_{ij}(\mathrm{I}_x) = \begin{cases} b_{ij} + c_{ij} \exp\left(-\sqrt{\mathrm{I}_x + 0.01}\right), & \text{for } i \neq j \\ 0, & \text{for } i = j \end{cases} \tag{8}$$

where $B_{ij}(\mathrm{I}_x) = B_{ji}(\mathrm{I}_x)$, and b_{ij} and c_{ij} are calculated as functions of temperature as

$$b_{ij} = b_{0,ij} + b_{1,ij}T + \frac{b_{2,ij}}{T} + \frac{b_{3,ij}}{T^2} + b_{4,ij} \ln T \tag{9}$$

$$c_{ij} = c_{0,ij} + c_{1,ij}T + \frac{c_{2,ij}}{T} + \frac{c_{3,ij}}{T^2} + c_{4,ij} \ln T \tag{10}$$

The model equations as well as the databank containing all the model parameters are implemented into a software package by OLI Systems Inc. The missing parameters in the system of our interest are obtained through a regression study using available experimental data such as solubility, heat capacity, and density. A variety of data is used in one single regression to ensure consistency of the model. The regression parameters are the UNIQUAC and the ion interaction parameters. Because the UNIQUAC parameters are primarily for non-electrolyte species, only the ion-ion and ion-molecule interactions are relevant to this work. After the determination of the missing parameters in the P_2O_5-$CaSO_4$-H_2O system, the MSE model can accurately predict gypsum solubility at a wide temperature range as shown in Fig. 2.

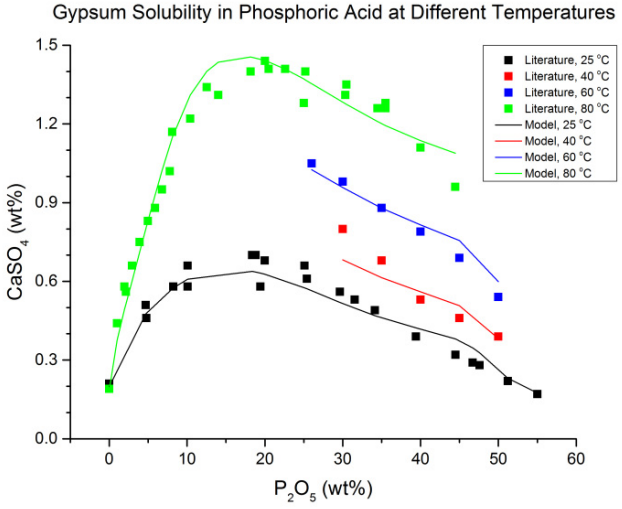

Fig. 2. Gypsum solubility in phosphoric acid at different temperatures

4.3. Supersaturation in electrolyte system

Accurate estimation of the solution supersaturation is critical in the measurement of crystal growth and nucleation kinetics. For multicomponent electrolyte systems, the relative supersaturation (σ) can be quantified by the dimensionless driving force for crystallization, which is the difference in chemical potential μ between supersaturated state and solid-liquid equilibrium state [22]:

$$\sigma = \frac{\mu_{\text{supersat}} - \mu_{\text{eq}}}{RT} = \ln\left(\frac{\prod_i a_i^{v_i}}{\prod_i a_{i,eq}^{v_i}}\right) = \ln\left(\frac{\prod_i a_i^{v_i}}{K_{\text{sp}}}\right) \tag{11}$$

where a_i is the activity of species i, v_i is the stoichiometric coefficient of species i, and K_{sp} is the solubility product defined as the product of all ion and molecules activities. For gypsum, the relative supersaturation is

$$\sigma = \ln\frac{a_{SO_4^{2-}} a_{Ca^{2+}} a_{H_2O}^2}{K_{\text{sp,gypsym}}} = \ln S \tag{12}$$

The key in estimating the supersaturation is to have a model that can accurately predict the activity coefficients, which has been often neglected in the previous studies [23–25]. In the past, each activity coefficient is usually assumed to be 1 or estimated using a relatively simple model such as the Debye-Hückel model, which is only valid in dilute solutions. More complicated thermodynamics models such as the Bromley model have been used in the estimation of supersaturation in barium sulfate crystallization [26]. The MSE model implemented in the OLI software is used in this study for calculating the activity coefficients and thus the gypsum relative supersaturation in the concentrated multicomponent electrolyte system.

4.4. Integrate OLI Engine into Matlab

The functionality of the OLI software is made possible in other programming environments by OLI Engine version 8.2, which is a collection of libraries that enables access to the OLI equilibrium calculation. The access to the OLI functionality was implemented in Excel Macro/VBA based on an example file provided by the OLI user manual. Since the MOC was solved in the Matlab environment, these Excel Macros were used as an intermediate that passes liquid-phase composition from the Matlab program to the OLI Engine. Once a thermodynamics calculation is triggered, the OLI engine returns speciation and supersaturation back to the Matlab program. To reduce the number of OLI Engine function calls, the equilibrium computation is only triggered when the change in the amount of gypsum crystallized is large enough (0.1%).

5. Impurity growth model

The presence of impurities can inhibit or promote a crystal face growth rate and thus can modify crystal habit [27]. The extent of the growth rate retardation or promotion on each crystal facet depends on the concentration of impurities, solution supersaturation, and temperature. Most of the earlier literature does not take into account the effect of impurity concentration on solubility and only reports the overall effect on growth rate, which may lead to an erroneous interpretation of the measured growth rate since the reference for equilibrium is different [28]. Our approach to study the effect of impurities is to first understand the effect of impurity on crystal solubility using the MSE model, and then study the effect of impurity on growth rate in L and W direction at controlled supersaturation.

A recent review on impurity growth model is available [chapter 4 of 29]. For a single impurity, the Kubota-Mullin growth model [30] is widely used. This model assumes that the impurity molecule adsorbs on the crystal surface

thereby reducing the number of available sites for crystal growth and, as a consequence, inhibits overall crystal growth rate by

$$\frac{G}{G_0} = 1 - \alpha\theta_{\text{eq}} \tag{13}$$

where G_0 is the growth rate without impurity and G is the growth rate with impurity present, α is the impurity effectiveness parameter which has a non-negative value, and θ_{eq} is the equilibrium surface coverage. The surface coverage by impurity may be described by adsorption isotherms such as Langmuir isotherms. Then the complete expression for Kubota-Mullin single impurity growth model is

$$\frac{G}{G_0} = 1 - \alpha\frac{Kc_I}{1+Kc_I} \tag{14}$$

where K is the adsorption constant and c_I is the impurity concentration.

The generalization of the Kubota-Mullin model to account for varying supersaturation and temperature [31,32] and multiple impurities adsorption [29] is

$$\frac{G}{G_0} = 1 - \left(\frac{\beta}{T\sigma}\right)\frac{Kc_I}{1+Kc_I} \tag{15}$$

where T is temperature in Kelvin, σ is relative supersaturation, and β is a parameter.

The Kubota-Mullin model for the adsorption of multiple impurities assumes all impurities compete for the vacant sites. For two competing impurities with a mixed Langmuir isotherm, the model is

$$\frac{G}{G_0} = 1 - \left(\frac{\beta}{T\sigma}\right)\frac{K_A c_A + K_B c_B}{1+K_A c_A + K_B c_B} \tag{16}$$

The impurity growth model can be used to model gypsum crystal growth in the presence of impurities and subsequently used in the general population balance modeling for the prediction of gypsum SSD. Experimental data for growth inhibition of gypsum due to some metal ions were reported in [33]. The reported kinetic data did not perform solubility analysis before carrying out growth inhibition experimental study. Nevertheless, these data were used as a preliminary test for the Kubota-Mullin model (15). The adjusted R^2 value in Table 1 indicates a fairly good model fit for impurity inhibition in gypsum crystal.

Table 1. Kubuta-Mullin model fit for gypsum in the presence of metal ion impurities using data from [33].

Metal ion impurity	Adjusted R^2	# of data points
Mg^{2+}	0.99	6
Cr^{3+}	0.96	6
Fe^{3+}	0.94	6
Cu^{2+}	0.95	6
Cd^{2+}	0.96	6
Cd^{2+} at varying supersaturation	0.85	18

6. Dynamic simulation of a seeded batch crystallization

In seeded batch crystallization, the crystallizer is initially charged with reactants and gypsum seed crystals. As the crystallization occurs, the level of supersaturation decreases until the solution reaches saturation. The objective of the seeded batch crystallization simulation is to predict the SSD in the system with and without impurity using the 2D PBM and the Kubuta-Mullin model. The solution nonideality is taken into account by the MSE model, which predicts the solution supersaturation given the composition. The missing coefficients in the MSE model for the P_2O_5-$CaSO_4$-H_2O chemical system are obtained from regression of gypsum solubility data. In this simulation, tricalcium phosphate ($Ca_3(PO_4)_2$) is used to represent phosphate rock in the Wet Process:

$$\mathrm{Ca_3(PO_4)_2 + 3\,H_2SO_4 + 6\,H_2O \longrightarrow 2\,H_3PO_4 + 3\,CaSO_4 \cdot 2H_2O\downarrow}$$

6.1. Crystallization simulation without impurity

The assumptions made in this simulation are:

- Reactants dissolve into aqueous form instantaneously
- Reaction is isothermal
- Only gypsum crystallizes
- Both solution and solid particles are well-mixed in the reactor
- Secondary nucleation is the only nucleation mechanism
- Growth rates in both *L* and *W* directions are size independent

These assumptions simplify the PBE (2) to

$$\frac{\partial f}{\partial t} + G_L \frac{\partial f}{\partial L} + G_W \frac{\partial f}{\partial W} = k_b \sigma^b \mu_3 \delta(L,W) \tag{17}$$

The algebraic mass balances for the gypsum reaction are

$$c_{\Delta gyp}(t) = \frac{k_v \rho}{\mathrm{MW}} \left(\mu_3(t) - \mu_3(0) \right) \tag{18}$$

$$c_{\mathrm{Ca_3(PO_4)_2}}(t) = c_{\mathrm{Ca_3(PO_4)_2}}(0) - \frac{1}{3} c_{\Delta gyp}(t) \tag{19}$$

$$c_{\mathrm{H_2SO_4}}(t) = c_{\mathrm{H_2SO_4}}(0) - c_{\Delta gyp}(t) \tag{20}$$

$$c_{\mathrm{H_2O}}(t) = c_{\mathrm{H_2O}}(0) - 2c_{\Delta gyp}(t) \tag{21}$$

$$c_{\mathrm{H_3PO_4}}(t) = c_{\mathrm{H_3PO_4}}(0) + \frac{2}{3} c_{\Delta gyp}(t) \tag{22}$$

$$\mu_3(t) = \mu_{3,\mathrm{seed}}(t) + \mu_{3,\mathrm{nuc}}(t) \approx \sum_j \sum_i f_{ij} L_i W_j^2 \Delta L_i \Delta W_i + \sum_k f_k L W^2 \sqrt{\Delta L_k^2 + \Delta W_k^2} \tag{23}$$

where ρ is crystal density (2.308 g/cm^3), and k_v is crystal shape factor (e.g., 1 for a square-shaped cross section). Combining these equations with the system of ODEs (4) from the MOC conversion results in a system of differential-algebraic equations of index 1, which can be easily solved using commercial solvers such as ode15s in Matlab. The associated parameters in the growth and nucleation models

$$G_W = k_{g_W} \exp\left(-\frac{E_{g_W}}{RT}\right)\sigma^{g_W}, \quad G_L = k_{g_L} \exp\left(-\frac{E_{g_L}}{RT}\right)\sigma^{g_L}, \tag{24}$$

$$B = k_b \exp\left(\frac{E_b}{RT}\right)\sigma^b \mu_3 \delta(L,W), \tag{25}$$

are measured from a series of MSMPR experiments and are reported in Table 2.

Table 2. Growth (24) and nucleation (25) model parameters for gypsum crystal without impurity.

parameters	L dimension	Units
k_{g_L}	5.76×10^5	μm/s
k_{g_W}	1.00×10^5	μm/s
E_{g_L}/R	5420	Kelvin
E_{g_W}/R	5030	Kelvin
g_W, g_L	2	dimensionless
k_b	1.50×10^3	#/(μm^3-s)
E_b/R	-6740	Kelvin
b	2	dimensionless

The seed crystal distribution has the form of a 2D Gaussian distribution with mean and standard deviation of 40 μm and 8 μm in both the L and W directions. The initial concentration of each compound in the solution is listed in Table 3. Other simulation parameters are listed in Table 4.

Table 3. Composition and supersaturation in the batch crystallization simulation at various time points.

States in the crystallizer	t = 0 s	t = 2100 s	t = 6000 s
$Ca_3(PO_4)_2$	0.01 mol	0.0083 mol	0.0069 mol
H_2SO_4	0.12 mol	0.115 mol	0.111 mol
H_2O	25 mol	24.990 mol	24.982 mol
H_3PO_4	0.01 mol	0.0133 mol	0.0162 mol
Seeded gypsum	3.0×10^{-4} mol	1.1×10^{-3} mol	1.2×10^{-3} mol
Nucleated gypsum	0 mol	4.2×10^{-3} mol	8.3×10^{-3} mol
Temperature	80°C	80°C	80°C
Supersaturation	1.489	1.248	1.038

Table 4. Simulation parameters.

Parameter	Value
# of characteristics for seeded crystals	20×20
# of characteristics for nucleated crystals	60 pre-allocated
Simulation time	6000s
relative error tolerance for ODE solver	1×10^{-3}
relative error tolerance for OLI software	1×10^{-6}
threshold that triggers OLI computation	0.1% in relative $\Delta\mu_3$
r_0	3 μm

6.2. Crystallization simulation with impurity

The presence of impurity is included in the 2D PBM to simulate the change in SSD in the batch reactive crystallization of gypsum. The simulation with impurity is based on the simulation without impurity except the inclusion of the Kubuta-Mullin growth inhibition model. Since parameters associated with the growth inhibition model for gypsum are not available for any impurity compound, a fictitious impurity with parameters in Table 5 is used in this simulation as to demonstrate the shape changing effect. Furthermore, the fictitious impurity is assumed to have no effect on the solution chemistry and supersaturation in this simulation. Although the last assumption does not hold in general, the MSE model can easily include the change in solution nonideality due to a known impurity compound. The impurity concentration is also assumed constant, as the amount absorbed on the crystal surface is relatively small compare to the bulk concentration of the impurity.

Table 5. Kubuta-Mullin model parameters for the fictitious impurity

Growth direction	β (Kevin)	K (M^{-1})	c_I (M)
L	800	1	0.025
W	500	0.5	0.025

7. Results and discussion

Snapshots of the time evolution of the crystal SSD and supersaturation without impurity at three different time points are shown in Fig. 3. The first snapshot (Fig. 3a) shows the 2D CSD of the initial seed crystals. The second and third snapshots were obtained after 2100 s and 6000 s of the simulation. The seeded CSD appears to be flat in Fig. 3bc due to the large amount of gypsum crystal nuclei, but actually has the same peak value as in Fig. 3a. The seeded CSD has the same shape as in Fig. 3a – just with different mean width and length. The rate of crystal formation is captured by the supersaturation profile. The rate of decrease in supersaturation is low at the beginning because the amount of crystals to grow on is small. As the total crystal mass (and external surface area) gains due to nucleation, the supersaturation drops sharply. When the supersaturation approaches the equilibrium state, both nucleation and growth slow. The composition and supersaturation at the three snapshots are in Table 6.

In Fig. 3, each point plotted in the supersaturation profile represents an OLI function call. The OLI function calls are most frequent when the rate of change of the supersaturation is the largest.

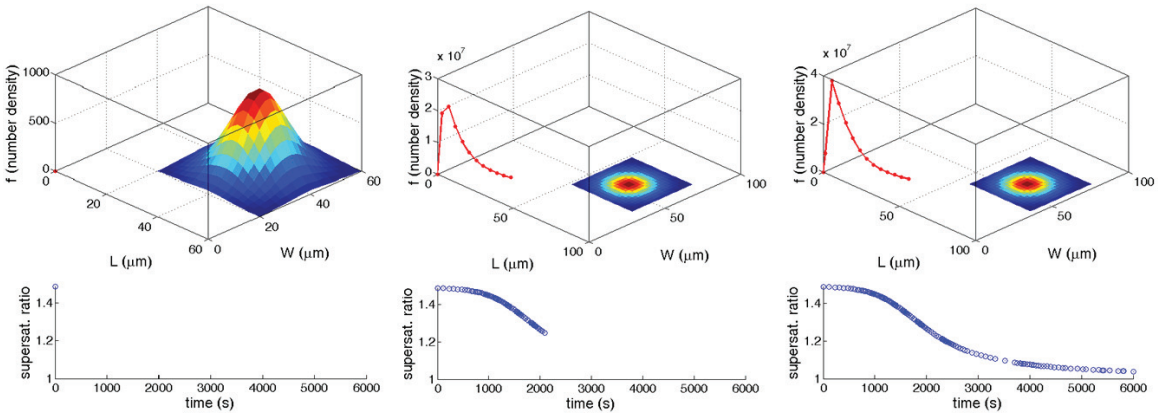

(a) t=0 s (b) t=2100 s (c) t=6000 s

Fig. 3. Dynamic simulation without impurity using kinetic parameters in Table 2, initial conditions in Table 4, and simulation parameters in Table 4. The top plots of are the 2D CSD at t = 0 s, t = 2100 s, and t = 6000 s obtained from solving (17) using the MOC. The bottom plots are the supersaturation profile obtained from the MSE model.

The simulations with impurity generate similar plots to Fig. 3. To illustrate the effect of the impurity on crystal SSD, the average crystal length, width, and aspect ratio (L/W) are plotted as function of time in Fig. 4. In both the system with and without impurity, the initial average L and W correspond to the mean L and W of the seeded crystal with an aspect ratio of 1. Comparing the average L and W profiles with and without impurity, the presence of impurity decreased average length L due to a stronger growth inhibition in the L direction. While in the W direction, the presence of impurity increased average width W due to higher supersaturation as a result of the retarded growth in the L direction outweighing the inhibition due to impurity in the W direction. In this simulation, the presence of impurity decreased the average aspect ratio from 1.9 to 1.2.

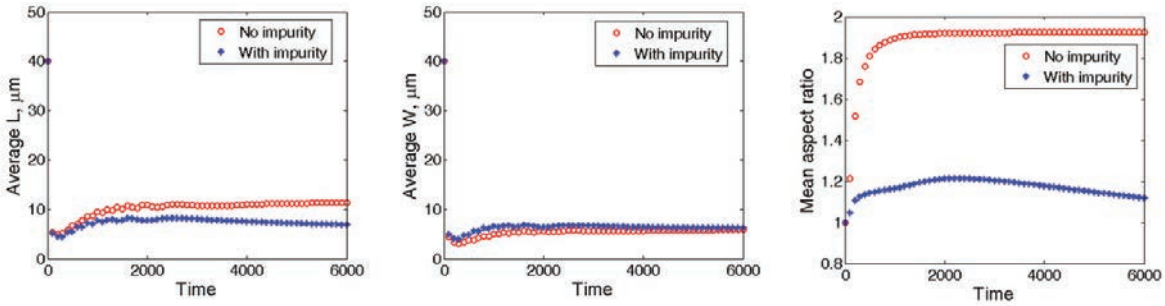

Fig. 4. The average crystal length, width, and aspect ratio from simulations with and without impurity.

8. Conclusion

The modelling framework presented in this article combines three models: (1) the MSE thermodynamic model that accounts for solution nonideality, (2) a 2D PBM that predicts the evolution of crystal SSD, and (3) the Kubuta-Mullin growth inhibition model that predicts the effect of impurity on crystal growth rate. The simulation results from the combined model framework demonstrate the capability of simulating gypsum crystal SSD in the presence of impurity in a nonideal aqueous solution composed of multiple species. Further, a computationally efficient 2D PBM solver based on the method of characteristics was developed and implemented in Matlab. To integrate the MSE model in the OLI software package to the Matlab environment, Excel Macros were developed to efficiently exchange data between the two models. Future experiments will be used to determine parameters in the growth inhibition model and validate simulation results.

Acknowledgements

This work was supported by the OCP Group.

References

[1] P. Becker, Phosphates and Phosphoric Acid: Raw Materials, Technology, and Economics of the Wet Process, Marcel Dekker, Inc., New York, 1989.
[2] S.I. Abu-Eishah, N.M. Abu-Jabal, Chem. Eng. J. 81 (2001) 231–250.
[3] E.A. Abdel-Aal, M.M. Rashad, H. El-Shall, Cryst. Res. Technol. 39 (2004) 313–321.
[4] W.E. Hunter, P.A. Rey, Method of Improving Gypsum Slurry Filtration in the Production of Phosphoric Acid, US5211928 A, 1993.
[5] H.M. Hulburt, S. Katz, Chem. Eng. Sci. 19 (1964) 555–574.
[6] A. Randolph, M.A. Larson, Theory of Particulate Processes: Analysis and Techniques of Continuous Crystallization, Academic Press, Inc., New York, 1988.
[7] D. Ramkrishna, A.W. Mahoney, Chem. Eng. Sci. 57 (2002) 595–606.
[8] P. Marchal, R. David, J.P. Klein, J. Villermaux, Chem. Eng. Sci. 43 (1988) 59–67.
[9] J. Hostomsky, A.G. Jones, J. Phys. D. Appl. Phys. 24 (1991) 165–170.
[10] J. Bakldyga, W. Podgórska, R. Pohorecki, Chem. Eng. Sci. 50 (1995) 1281–1300.

[11] H. Muhr, R. David, J. Villermaux, P. Jezequel, Chem. Eng. Sci. 51 (1996) 309–319.
[12] C.B.B. Costa, M.R.W. Maciel, R.M. Filho, Comput. Chem. Eng. 31 (2007) 206–218.
[13] A.H. Alexopoulos, A.I. Roussos, C. Kiparissides, Chem. Eng. Sci. 59 (2004) 5751–5769.
[14] G. Azimi, V.G. Papangelakis, Fluid Phase Equilib. 290 (2010) 88–94.
[15] G. Azimi, V.G. Papangelakis, J.E. Dutrizac, Fluid Phase Equilib. 266 (2008) 172–186.
[16] G. Azimi, V.G. Papangelakis, J.E. Dutrizac, Fluid Phase Equilib. 260 (2007) 300–315.
[17] P. Wang, A. Anderko, R.D. Springer, R.D. Young, J. Mol. Liq. 125 (2006) 37–44.
[18] S.I. Sandler, editor, Models for Thermodynamic and Phase Equilibria Calculations, Marcel Dekker, New York, 1995.
[19] P. Wang, A. Anderko, R.D. Young, Fluid Phase Equilib. 203 (2002) 141–176.
[20] K.S. Pitzer, G. Mayorga, J. Phys. Chem. 77 (1973) 2300–2308.
[21] H. Helgeson, D. Kirkham, Am. J. Sci. 273 (1974) 1089–1198; 274 (1974) 1199–1261.
[22] J. Newman, K. E. Thomas-Alyea, Electrochemical Systems, third ed., Wiley, Hoboken, NJ, 2004.
[23] M. El Moussaouiti, R. Boistelle, A. Bouhaouss, J.P. Klein, Chem. Eng. J. 68 (1997) 123–130.
[24] S.-T. Liu, G.H. Nancollas, J. Cryst. Growth 6 (1970) 281–289.
[25] E.T. White, S. Mukhopadhyay, ACS Symp. Ser. 438 (1990) 292–315.
[26] H. Wei, J. Garside, Chem. Eng. Res. Des. 75 (1997) 219–227.
[27] K. Sangwal, Prog. Cryst. Growth Charact. Mater. 32 (1996) 3–43.
[28] G. Fevotte, N. Gherras, J. Moutte, Cryst. Growth Des. 13 (2013) 2737–2748.
[29] K. Sangwal, Additives and Crystallization Processes: From Fundamentals to Applications, John Wiley & Sons, Chichester, UK, 2007.
[30] N. Kubota, J.W. Mullin, J. Cryst. Growth 152 (1995) 203–220.
[31] N. Kubota, M. Yokota, J.W. Mullin, J. Cryst. Growth 182 (1997) 86–94.
[32] N. Kubota, M. Yokota, J.. Mullin, J. Cryst. Growth 212 (2000) 480–488.
[33] S.K. Hamdona, U.A. Al Hadad, J. Cryst. Growth 299 (2007) 146–151.